Solution Structure of a Band 3 Peptide Inhibitor Bound to Aldolase: A Proposed Mechanism for Regulating Binding by Tyrosine Phosphorylation[†,‡]

Michael L. Schneider and Carol Beth Post*

Department of Medicinal Chemistry, Purdue University, West Lafayette, Indiana 47907-1333

Received July 18, 1995; Revised Manuscript Received October 20, 1995[⊗]

ABSTRACT: Human erythrocyte band 3 inhibits glycolytic enzymes, including aldolase, by binding these cytoplasmic enzymes at its N-terminus. Phosphorylation of Y8 disrupts inhibition, and there is evidence that *in vivo* glycolysis levels in erythrocytes are regulated in part by a phosphorylation/dephosphorylation signaling pathway. The structural basis for control by phosphorylation has been investigated by NMR studies on a complex between aldolase and a synthetic peptide corresponding to the first 15 residues of band 3 (MEELQDDYEDMMEEN-NH_2). The structure of this band 3 peptide (B3P) when it is bound to rabbit muscle aldolase was determined using the exchange-transferred nuclear Overhauser effect (ET-NOE). Two hundred NMR structures for B3P were generated by simulated annealing molecular dynamics with NMR-derived distance restraints and excluding electrostatic terms. Twenty structures were further refined against a force field including full partial charges. The important conformational feature of B3P in the bound state is a folded loop structure involving residues 4−9 and M12 that surrounds Y8 and is stabilized by a hydrophobic cluster with the ring of Y8 sandwiched between the methyl groups of L4 and M12. Differential line broadening indicates that this loop structure binds aldolase in a relatively specific manner, while terminal regions are structurally heterogeneous. To better understand B3P inhibition of aldolase and the mechanism of phosphorylation control, a complex was modeled by docking B3P into the active site of aldolase and optimizing the fit using restrained molecular dynamics and energy minimization. The B3P loop is complementary in conformation to the β-barrel central core containing the aldolase active site residues. Binding is electrostatic in nature with numerous ionic and hydrogen-bonding interactions involving several conserved lysine and arginine residues of aldolase. How phosphorylation of band 3 could disrupt inhibition was considered by modeling a phosphoryl moiety onto Y8 of B3P. An energetic analysis with respect to rigid phosphate rotation suggests that aldolase inhibition is reversed primarily because of electrostatic repulsion between B3P residues that destabilizes the B3P loop formed in the complex. This proposed intramolecular mechanism for blocking protein−protein association by electrostatic repulsion with the phosphoryl group may be applicable to other protein−protein signaling complexes.

The human erythrocyte anion transporter, band 3, has been shown to tightly bind and inhibit three enzymes essential for carrying out glycolysis (Low, 1986; Salhany, 1990): aldolase (Strapazon & Steck, 1976; Murthy et al., 1981), glyceraldehyde-3-phosphate dehydrogenase (GAPDH),[1] and phosphofructokinase (PFK) (Tsai et al., 1982; Jenkins et al., 1984). Binding of these enzymes is highly specific for the N-terminus in the cytoplasmic domain since the removal of the N-terminus of band 3 prevents binding (Low, 1986). Phosphorylation of tyrosine 8 reverses the inhibition of aldolase, GAPDH, and PFK and allows these enzymes to regain full catalytic activity (Low et al., 1987; Harrison et al., 1991). Y21 is also phosphorylated (Harrison et al., 1994) but to a lesser degree and is therefore thought to be less functionally important.

It is believed that tyrosine phosphorylation of band 3 at position 8 modulates the interaction between band 3 and the glycolytic enzymes *in vivo*. Evidence that band 3 can regulate erythrocyte glycolysis *in vivo* was obtained by demonstrating (Rogalski et al., 1989; Harrison et al., 1991; Low et al., 1993) that glycolytic rates in intact erythrocytes are elevated under conditions that stimulated tyrosine phosphorylation in band 3 or when the N-terminus of band 3 is blocked by antibodies. In addition, Y8 has been shown to be a substrate for band 3 tyrosine kinase (Mohamed et al., 1986; Boivin et al., 1986), which is now thought to be endogenous $p72^{syk}$ (Harrison et al., 1994), and there is evidence that red cell acid phosphatase will dephosphorylate Y8, subsequently restoring band 3 protein's inhibitory properties (Boivin & Galand, 1986). Together, it has been suggested that these features support a new type of metabolic control that is neither covalent modification of the regulatory enzyme nor metabolite modulation, whereby erythrocyte glycolysis is regulated through a protein tyrosine kinase/phosphatase system that modulates the formation of an

[†] This research was supported by an NIH award (GM39478), an NIH Biophysics Training Grant (GM08296) fellowship received by M.L.S., and funding from the Lucille P. Markey Foundation.

[‡] The atomic coordinates have been deposited in the Brookhaven Protein Data Bank and assigned the identity codes 2BTA and 2BTB.

[⊗] Abstract published in *Advance ACS Abstracts,* December 1, 1995.

[1] Abbreviations: GAPDH, glyceraldehyde-3-phosphate dehydrogenase; PFK, phosphofructokinase; *syk*, spleen tyrosine kinase; B3P, band 3 peptide; ET-NOE, exchange-transferred nuclear Overhauser effect; *t*-boc, *tert*-butyloxycarbonyl; f-moc, 9-fluorenylmethyloxycarbonyl; HPLC, high-performance liquid chromatography; FPLC, fast-performance liquid chromatography; TFA, trifluoroacetic acid; FAB-MS, fast atom bombardment mass spectrometry; ET-NOESY, exchange-transferred nuclear Overhauser effect spectroscopy; TOCSY, total correlation spectroscopy; ROESY, rotating Overhauser effect spectroscopy; SA, simulated annealing; cpu, central processing unit; DHAP, dihydroxyacetonephosphate; rmsd, root mean square deviation; B3PALD, band 3 peptide−aldolase model complex; SH, *src* homology region.

0006-2960/95/0434-16574$09.00/0

inhibitory complex (Low et al., 1993). What actually triggers this phosphorylation/dephosphorylation event remains to be discovered.

To better understand the regulatory action of band 3, ^{1}H NMR structural studies were carried out using a synthetic N-terminal pentadecapeptide of residues 1−15 of band 3. The sequence according to Tanner et al. (1989) is MEELQDDYEDMMEEN. This band 3 peptide (B3P) is a good model for inhibition by band 3 since it is known to tightly bind to aldolase and inhibit catalysis (Strapazon et al., 1977; Low, 1986; Harrison et al., 1991). We describe in this paper the determination and analysis of the unphosphorylated B3P conformation in the B3P−aldolase complex. The bound B3P structure was determined by utilizing the exchange-transferred nuclear Overhauser effect (ET-NOE), the transfer of the NOE magnetization developed between B3P protons in the bound ligand state to the unbound ligand resonances via chemical exchange (Balaram et al., 1973; Clore et al., 1982, 1983; Campbell & Sykes, 1993; Ni, 1994; Murali et al., 1994). The versatility of the ET-NOE makes it a valuable technique for studying molecular interactions in biological systems.

A mechanism for modulating protein−protein interactions via tyrosine phosphorylation is proposed on the basis of the structure of a B3P−aldolase complex modeled from the coordinates of B3P determined by NMR and of aldolase determined by X-ray crystallography (Gamblin et al., 1990). An energetic analysis of the complex elucidates two features that appear to be important for regulation by phosphorylation. First, the formation of the complex is prevented by phosphorylation largely as a result of repulsive electrostatic interactions, as opposed to unfavorable steric ones, between residues of band 3. Second, other charged residues of B3P interact with aldolase and are responsible for the recognition of binding. This mechanism for phospho−tyrosyl modulation of protein−protein association, in which intramolecular interactions upon phosphorylation block association, could hold for the other band 3−glycolytic enzyme complexes or, even more generally, for other protein−protein signaling complexes.

MATERIALS AND METHODS

Peptide and Aldolase Preparation. The band 3 peptide (MEELQDDYEDMMEEN-NH_2) was synthesized by the Purdue University Peptide Synthesis Facility using solid-phase synthesis. Both *t*-boc and f-moc amino acid derivatives were used in separate syntheses, and the C-terminus of B3P was amidated. Although the N-terminus is acetylated in native band 3, B3P was synthesized without the acetyl group to increase the exchange rate between the bound and unbound state and facilitate ET-NOE measurements (Murthy et al., 1981; Wang et al., 1992). Reverse-phase HPLC and Pharmacia's FPLC system were used for purification and desalting. A Rainin Dynamax 300A column (10 mm × 25 cm, C_{18}, 12 μm silica particle size) and a Pharmacia preparatory column (25 mm × 15 cm, C_2−C_{18}, 15 μm silica particle size) were used for separation using a solvent system of 0.1% TFA in H_2O and 0.1% TFA in 95% HPLC-grade acetonitrile/5% H_2O. Fractions were detected at 215 nm, and fast atom bombardment mass spectrometry (FAB-MS) was used to confirm the correct mass in the fraction corresponding to B3P.

Rabbit muscle aldolase was purchased as a crystalline suspension from Sigma. It was dialyzed overnight in 10 mM phosphate, pH 5.5 at 4 °C, for all experiments requiring aldolase.

K_d and k_{off} Determination. The dissociation constant K_d was derived from an aldolase inhibition assay using B3P as the inhibitor (Schneider et al., unpublished results). From steady-state kinetics, a K_d value of 5.2×10^{-6} M at pH 5.5, 10 mM phosphate, and 25 °C was determined. In addition, competitive inhibition was observed for aldolase in the presence of B3P, as was observed in the presence of band 3 (Murthy et al., 1981).

The interpretation of ET-NOESY data is facilitated when ligand binding is in the fast-exchange limit (Clore et al., 1983; Lee & Krishna, 1992; London et al., 1992; Ni, 1994) specified by a dissociation rate, k_{off}, much greater than the cross-relaxation rate. Assuming diffusion-limited binding, k_{off} may be approximated from $K_d k_{on}$, where k_{on} is the bimolecular association rate constant. The value for k_{on} is taken to be 10^8 M^{-1} s^{-1}, somewhat lower than diffusion limited (Espenson, 1981) since B3P is a relatively large ligand, giving an estimate for k_{off} of 520 s^{-1}. Since the cross-relaxation rates for a molecular mass of 160 kDa are approximated to be <50 s^{-1}, B3P binding is in the fast-exchange limit.

NMR Spectroscopy and Sample Preparation. All ^{1}H spectra were obtained at 11.7 T using a Varian VXR-500 spectrometer at a probe temperature of 25 °C and a 6000 Hz spectral width. The NMR experiments were carried out on 0.7 mL samples of 2.8 mM B3P in the absence or presence of 70 μM aldolase. In addition, all samples contained 10 mM potassium phosphate at pH 5.5, made up with either 99.996% D_2O (Isotec, Inc.) or 90% H_2O/10% D_2O. The mole ratio of B3P to aldolase subunit was 10:1 for samples containing aldolase, and pH values were uncorrected for deuterium isotope effects. Specificity for B3P binding to aldolase was checked by adding 26 mM lithium salt of dihydroxyacetone phosphate (DHAP) (Sigma) to a B3P−aldolase sample and comparing to a control sample with 26 mM potassium phosphate added to give approximately the same ionic strength. All 2D spectra were acquired in a phase-sensitive mode using the method of States et al. (1982) for quadrature detection. Varian's VNMR 3.1 software package on a SUN Sparc 1^+ workstation was used for all spectral processing. For two-dimensional spectra, Gaussian apodization in both dimensions and zero-filling were used to generate 4K × 4K data sets from NMR samples containing no aldolase and 2K × 2K data sets from NMR samples containing aldolase. Presaturation with the decoupler channel or transmitter channel was used for the 90% H_2O samples, and recycle times ranged from 2 to 3 s. TOCSY (Braunschweiler & Ernst, 1983; Bax et al., 1985), ROESY (Bothnerby et al., 1984; Kessler et al., 1987), and NOESY (Jeener et al., 1979; Macura & Ernst, 1980) spectra were acquired for NMR samples lacking aldolase. TOCSY spectra utilizing the MLEV-17 mixing sequence and mixing times of 30 and 70 ms were used to identify the ^{1}H spin systems, and ROESY spectra with a 300 ms mixing time were used to make sequential assignments. For all spectra of B3P in the free state, 512 hypercomplex t_1 increments were collected with 4K points during the acquisition period (t_2 dimension) and 16 transients per increment. ET-NOESY spectra of the B3P−aldolase complex contained 256 hyper-

complex t_1 increments and 2K points in the t_2 dimension with 32 transients per increment. ET-NOESY with mixing times of 150 and 200 ms in 90% H_2O and 150 ms in D_2O were measured for aldolase−B3P and 150 ms for B3P in the absence of aldolase.

NMR Structure Determination. NOE distance restraints, classified as strong (1.8−2.7 Å), medium (1.8−3.3 Å), or weak (1.8−5.0 Å), were derived by counting contours of ET-NOESY cross-peaks and categorized using the intensity of cross-peaks between $H_{\delta 1+\delta 2}$ and $H_{\epsilon 1+\epsilon 2}$ protons of tyrosine 8 as a reference. In order to scale the ET-NOE's measured in 90% H_2O to those measured in D_2O, the ratio of the Y8 $H_{\delta 1+\delta 2}$ and $H_{\epsilon 1+\epsilon 2}$ cross-peak intensity in the D_2O spectrum to that in the H_2O spectrum was used to weight all cross-peaks in the 90% H_2O ET-NOESY spectrum. Additional restraints were included to improve the efficiency of the conformational search. Fourteen ϕ dihedral angle restraints with a broad minimum ($-180° \leq \phi \leq -30°$), corresponding to the acceptable region of a Ramachandran plot, were used to maintain all ϕ angle values in the realm normally observed in proteins. Extensive packing interactions, which greatly facilitate structure determination of larger proteins, are not present for a peptide. Thus, without extensive packing interactions we found that standard simulation protocols (see below) were not efficient for sampling the larger conformational space accessed by a peptide and lead to a large number of peptide structures with poor geometry. Even though these ϕ restraints helped convergence, they are not necessary for defining the final NMR structures. To show that the ϕ restraints are not a determinant of the structural solution, a protocol without ϕ restraints that included 5 ps of distance-restrained simulated annealing and a final 150 steps of distance-restrained Powell minimization was applied to a random selection of the final 20 NMR structures. The changes in the ϕ angles were insignificant, and the backbone (N, C_α, C) rmsd between the structures obtained with and without ϕ restraints was less than or equal to 0.72 Å.

Restrained molecular dynamics with the program X-PLOR 3.1 (Brünger, 1992) was used for structure determination of B3P. Initial coordinates from very dissimilar structures, either a right-handed α-helix or an extended coil, were used to remove possible bias from the initial configuration in the sampling of conformational space. The simulated annealing protocol was as follows: high-temperature dynamics for 30 ps with 1 fs time steps and temperature coupling to 1000 K; lowering the temperature to 100 K at a linear rate for 15 ps; 1200 steps of Powell minimization. A soft square-well potential was used for the distance and dihedral angle restraints throughout the above procedure. The distance restraint force constant was maintained at 50 kcal mol^{-1} $Å^{-2}$ throughout, while the force constant for the dihedral angle restraints was 5 kcal mol^{-1} rad^{-2} during the high-temperature dynamics and was then increased to 200 kcal mol^{-1} rad^{-2} during the cooling period. The X-PLOR force field defined by topallhdg.pro and parallhdg.pro files was used in the SA protocol. A purely repulsive van der Waals term was used for the simulated annealing and minimization procedures. Neither an electrostatic term nor a full Lennard-Jones potential was used in the SA calculation. Two hundred B3P structures were generated with this protocol.

Twenty of the 200 structures were selected on the basis of a total energy evaluation and few NOE distance violations for further energy minimization using the all-hydrogen force field from CHARMM version 22 (MacKerrel et al., 1992; A. D. MacKerrel, Jr., and M. Karplus, to be submitted for publication) and a full Lennard-Jones potential and electrostatic Coulombic potential. Modifications were made to the topallh22x.pro and parallh22x.pro files in the X-PLOR library to add improper angles and the corresponding force constants to maintain tyrosine ring planarity. This CHARMM force field was chosen for final minimization since the X-PLOR force field defined by the topallhdg.pro and parallhdg.pro files used for simulated annealing and NMR-derived restraint terms includes unusually high force constants and special improper terms. A total of 2000 steps of Powell minimization were performed on the 20 structures using the CHARMM force field. $^1H-^1H$ distances and ϕ dihedral angles were restrained by a square-well potential and a force constant of 50 kcal mol^{-1} $Å^{-2}$ for distances or 200 kcal mol^{-1} rad^{-2} for dihedral angles.

Docking of the B3P NMR Structure with Aldolase. A model complex was made by docking the B3P coordinates obtained from NMR structure determination with the active site region of human muscle aldolase. The coordinates for human muscle aldolase were obtained from the Brookhaven Protein Data Bank (1ALD), and hydrogens were built onto heavy atoms according to geometry and hydrogen-bonding considerations. Coordinates for the enzyme isolated from rabbit muscle (Sygusch et al., 1985, 1987) were not available from the Data Bank; however, amino acid sequence identity between rabbit muscle and human muscle forms is 97.7% (Malek et al., 1988). The segment with residues 4 through 9 from the average of the final 20 structures of B3P was manually docked into the active site region of aldolase using QUANTA 4.0. This complex served as a reference coordinate set in docking individual structures. Each of the final 20 NMR structures of B3P were docked into the active site by superimposing the backbone atoms (N, C_α, C) of the B3P structure with the reference coordinate set of the manually docked average peptide structure. Each complex was then subjected to high-temperature molecular dynamics calculations and energy minimization to improve the modeled fit. CHARMM version 23 (Brooks et al., 1983) was used for the restrained minimization and dynamics procedure as follows: 150 steps of steepest descent minimization followed by 300 steps of Powell minimization in order to alleviate any situations that could lead to a high energy complex (i.e., poor side-chain geometry in the X-ray coordinates of aldolase as well as intramolecular and intermolecular close contacts); 5 ps dynamics using a 1 fs time step at an initial temperature of 500 K and slow cooling to a final temperature of 300 K; 150 steps of Powell minimization. Electrostatic terms and a full Lennard-Jones potential as well as NMR distance restraints and ϕ dihedral angle restraints for B3P were used throughout the above procedure. A soft square-well potential was used for the distance restraints while the ϕ dihedral angles were harmonically constrained. During the entire minimization and dynamics routines, the distance restraint force constant was maintained at 100 kcal mol^{-1} $Å^{-2}$, while the ϕ dihedral angles were constrained with a force constant of 100 kcal mol^{-1} rad^{-2}. All aldolase backbone atoms were harmonically constrained using a force constant of 100 kcal mol^{-1} $Å^{-2}$ during minimization and dynamics, and aldolase side-chain atoms were fixed during the dynamics simulation except those within a 10 Å radius from any B3P atom. Fixing side-chain atoms of aldolase was performed to

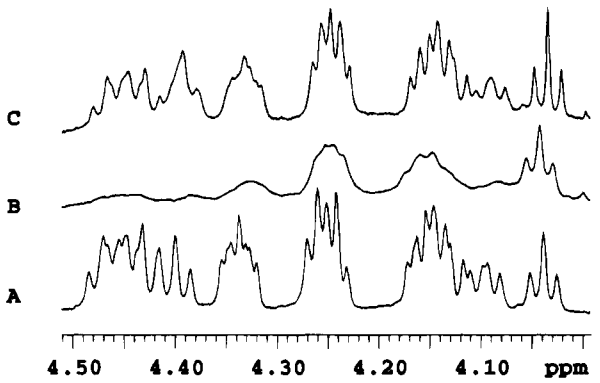

FIGURE 1: 1D ^{1}H NMR spectra showing the H_α region of 2.8 mM B3P in the free state (A), in the presence of 70 μM aldolase and added 26 mM phosphate (B), and in the presence of 70 μM aldolase and 26 mM DHAP (C). B3P binding to aldolase is specific since addition of DHAP, which is specific for the aldolase active site, reverses the broadening of B3P resonances by aldolase. The narrowed B3P line widths in (C) are the result of DHAP displacing B3P from aldolase (2.8 mM B3P, 10 mM PO_4, pH 5.5, 25 °C).

conserve cpu time during the dynamics portion of the docking procedure.

Another molecular docking approach was attempted which was less successful than the above methodology. Similar to the above protocol, the average structure was manually docked to the active site of aldolase. Unlike the above protocol, a family of complexes was generated from this single average structure, instead of superimposing each of the 20 final NMR structures onto the average structure. However, the structures generated had higher NOE violations and poorer geometry than those resulting from directly docking the 20 individual structures.

RESULTS

Sequential Resonance Assignments of B3P. Sequential assignments of B3P were made according to established procedures (Wuthrich et al., 1982; Billeter et al., 1982; Wagner & Wuthrich, 1982). TOCSY spectra were used to assign the ^{1}H side-chain spin systems of B3P. Sequential $H_{\alpha(i)}-H_{N(i+1)}$ and some intraresidue side-chain ROE interactions were observed. No other interresidue interactions were observed in either ROESY or NOESY spectra. Chemical shifts for all B3P ^{1}H resonances in the presence of aldolase are virtually identical except for Y8 ring resonances, $H_{\delta 1+\delta 2}$ and $H_{\epsilon 1+\epsilon 2}$; both shift upfield by 0.02 ppm.

Specificity of B3P Binding to Aldolase and Transferred NOE Results. Binding specificity is always a concern when measuring ET-NOE's, especially since it has been shown that nonspecific binding can occur at high ligand concentrations (Murali et al., 1993). Binding specificity of B3P for aldolase was shown by adding the aldolase inhibitor dihydroxyacetone phosphate (DHAP) (Mehler & Bloom, 1963) (also a product from the reversible cleavage of fructose 1,6-bisphosphate by aldolase) to a ^{1}H NMR sample containing B3P and aldolase. DHAP reverses the effect of aldolase on the B3P line widths and NOEs. Figure 1 shows the narrow resonances of free B3P (A) and the significantly broadened ones in the presence of aldolase and added phosphate (B). Upon addition of DHAP to a B3P−aldolase sample (C), B3P resonances narrow to closely resemble those observed in the free B3P spectrum. Similarly, the large increase in NOE intensities of B3P in the presence of aldolase is eliminated by addition of DHAP (data not shown). Since DHAP is specific for the active site of aldolase, these results show specificity of binding for B3P to aldolase. The B3P binding site on aldolase is discussed in more detail in the Discussion.

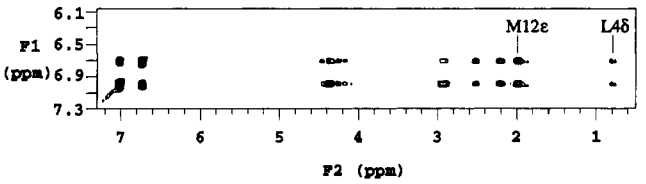

FIGURE 2: A strip from the aromatic region of the 500 MHz ET-NOESY spectrum showing intra- and interresidue ET-NOE's involving the Y8 ring protons of B3P bound to aldolase. Interactions important to structure determination are indicated between $H_{\delta 1+\delta 2}$ or $H_{\epsilon 1+\epsilon 2}$ of Y8 and the methyl groups of L4 and M12. The mole ratio of B3P to aldolase monomer is 10:1 (2.8 mM B3P, 70 μM aldolase, 100% D_2O, 10 mM PO_4, pH 5.5, 25 °C, mixing time 150 ms).

Figure 2 is a section of the 2D ET-NOESY spectrum of B3P and aldolase. As previously mentioned, B3P in the unbound state has negligible cross-relaxation so that the cross-peak intensities arise from the bound state of B3P. Furthermore, intermolecular NOE's between B3P and aldolase as well as intramolecular NOE's of aldolase are not observed due to the relatively long correlation time of aldolase causing ^{1}H line widths too broad to be discernible from the baseline.

Several important interresidue ET-NOE's involving the aromatic protons of Y8 are observed in Figure 2 for B3P in the presence of 0.1 molar equiv of aldolase subunit. Of particular importance to the tertiary structure determination of B3P are ET-NOE's seen between Y8 $H_{\delta 1+\delta 2}$ or $H_{\epsilon 1+\epsilon 2}$ and the methyl group protons of L4 or M12. In addition, interresidue interactions including weak $H_{\alpha(i)}-H_{\alpha(i+1)}$ ET-NOE's between Q5 and D6 and weak $H_{N(i)}-H_{N(i+1)}$ interactions between Y8 and E9 further defined the tertiary structure of B3P. Helical secondary structure is ruled out due to the lack of $i-i+3$ connectivities that would be present. The predominant ET-NOE's observed in the terminal portions of bound B3P were $H_{N(i)}-H_{\alpha(i+1)}$ connectivities except for a very weak $H_{\alpha(i)}-H_{\alpha(i+1)}$ ET-NOE observed between E14 and N15 as well as a weak $H_{N(i)}-H_{N(i+1)}$ contact between E13 and E14. There are few ET-NOE's to define the structure of the termini. This lack of ET-NOE's is due either to particular packing interactions having few short ^{1}H−^{1}H distances or to structural heterogeneity in binding band 3 peptide, giving a high degree of mobility in the terminal portions of B3P.

Structure Determination of B3P in the Bound State. Structure determination of B3P when bound to aldolase depended on a set of 68 *structurally significant* interproton distance restraints comprising 37 intraresidue, 15 sequential ($|i - j| = 1$), and 16 medium ($1 < |i - j| \leq 4$) range interresidue distances. By far, the largest number of NOE's involved Y8 with 26 NOE's and L4 with 15 NOE's. The total number of ET-NOE's observed exceeds 68, but extensive resonance overlap due to the amino acid content of B3P (i.e., 8 acidic residues out of 15) prevented utilization of additional ET-NOE's, most of which were intraresidue. We note that the uninterpreted cross-peaks likely would not have yielded additional distance information useful for structure determination since most of the overlapped cross-

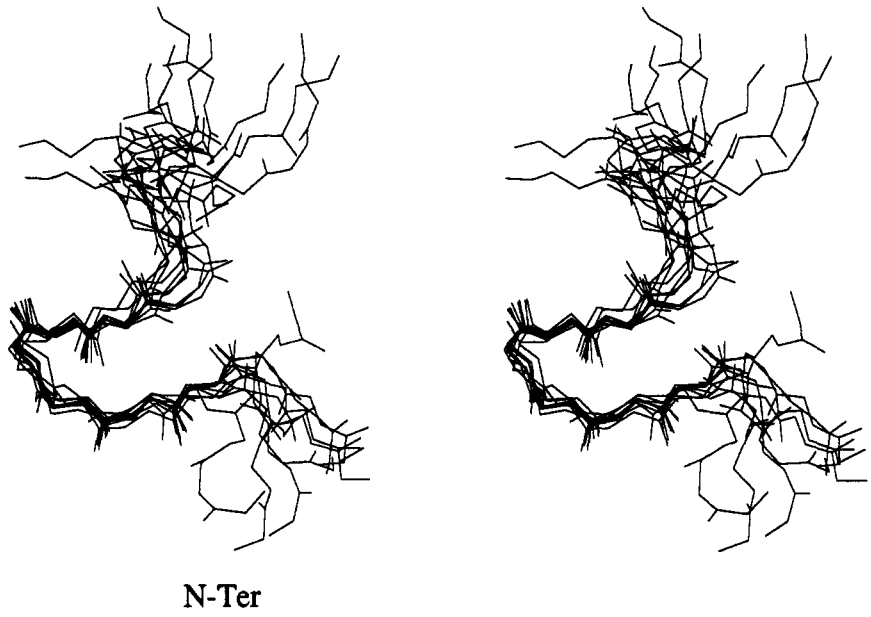

FIGURE 3: Superimposed stereoview of 10 of the 20 final calculated structures of B3P when bound to aldolase. The final 20 structures were selected from a set of 200 structures on the basis of the lowest total energy and lowest number of NOE violations. The well-defined loop comprises residues 4 through 9 (pairwise rmsd 1.21 ± 0.5 Å) while the terminal portions are more conformationally heterogeneous in the bound state.

peaks arise from vicinal proton interactions. Nevertheless, enough information was gathered to define the B3P structure. The distance restraints were derived by counting contours of the cross-peaks and classified as strong (1.8−2.7 Å), medium (1.8−3.3 Å), or weak (1.8−5.0 Å) in relative intensity. Although spin diffusion is always of concern, intermolecular spin diffusion is often negligible for short mixing times except for a few cases (Zheng & Post, 1993; Ni & Zhu, 1994). Furthermore, inherent errors such as spin diffusion are assumed in using the strong, medium, weak method for defining distance restraints (Post et al., 1990; Clore et al., 1993).

Structure determination proceeded by restrained molecular dynamics, including simulated annealing, and energy minimization with distance restraints and ϕ dihedral restraints as described in Materials and Methods. A total of 200 structures were generated with 100 structures derived from an initial α-helical structure and 100 structures derived from an initial extended chain. No distinction was found between the two sets of 100 structures. Twenty structures were selected on the basis of a combination of total energy less than 2.5 kcal/mol using the X-PLOR force field and zero NOE violations with a 0.1 Å cutoff since the number of violations alone was not enough of a selection criterion. Realizing that these selection criteria may not be optimal for selecting structures, work is in progress to develop a more rigorous analysis. The energy of the 20 structures was minimized further by utilizing the more accurate CHARMM force field and the NMR restraints. The final structures were well-behaved with respect to the NOE restraints, with the average number of NOE violations greater than 0.1 Å being 3.5 and no violations greater than 0.2 Å. The small increase in the number of NOE violations after energy minimization using the CHARMM22 force field may be due to the inclusion of electrostatics for this highly negatively charged peptide in the absence of solvent. Furthermore, van der Waals contacts and electrostatic interactions were favorable, leading to a mean total energy of −151.89 kcal/mol over the final 20 structures. The average of the pairwise rmsd values for the family of 20 structures calculated after superpositioning the main-chain atoms (N, C_α, and C) of residues 4 through 9 was 1.21 ± 0.5 Å. However, the pairwise rmsd for all main-chain atoms was 4.01 ± 1.4 Å, indicating disorder in the terminal portions of B3P as discussed in more detail in the following sections.

Structural Characteristics of Bound B3P. Figures 3 and 4 show a subset of the final 20 structures and the energy-minimized average B3P structure when bound to aldolase, respectively. As shown in Figure 4, the peptide is folded around Y8 while the side-chain carboxylates of D6, D7, and E9 extend out from the loop forming a negatively charged outer surface in the bound B3P molecule. This is not surprising since it has been shown that binding is largely electrostatic in nature (Strapazon & Steck, 1977). The loop in B3P is stabilized by a small hydrophobic cluster composed of the L4 methyl groups, the aromatic ring of Y8, and the M12 methyl group (Figure 4). The terminal portions of the peptide are disordered in comparison to the well-defined middle portion encompassing residues 4 through 9 (Figure 3). The structural heterogeneity in these sections of the peptide can be partly attributed to weak interaction with aldolase (see Discussion). Whether or not the structural heterogeneity occurs for the natural complex between the whole cytoplasmic domain of band 3 and aldolase is open to question.

Differential Line Broadening. Differential broadening of certain B3P resonances indicates which residues interact more strongly with aldolase. The magnitude of line broadening for a given resonance is proportional to the effective correlation time experienced by that residue of B3P. For instance, a resonance that is narrow compared with other resonances in the spectrum has a shorter effective correlation time due to greater mobility in the bound state, meaning that this residue does not interact as strongly with aldolase compared with other portions of B3P. Figure 5 shows 1D ^{1}H NMR spectra of B3P in the absence or presence of 0.1

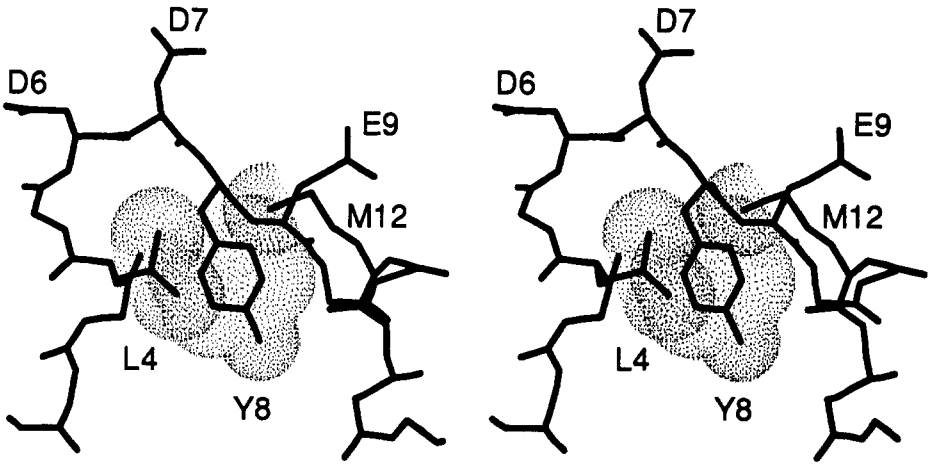

FIGURE 4: Energy-minimized average structure of B3P bound to aldolase. Coordinates were averaged over the final 20 NMR structures and then energy minimized including NMR restraints. Side-chain atoms are drawn for labeled residues only. L4, Y8, and M12 form a hydrophobic core within the well-defined loop, and van der Waals radii (dotted surfaces) show the ring of Y8 sandwiched between the side chains of L4 and M12. The side-chain carboxylates of D6, D7, and E9 point outward from the loop and form a negatively charged outer surface which directly interacts with aldolase.

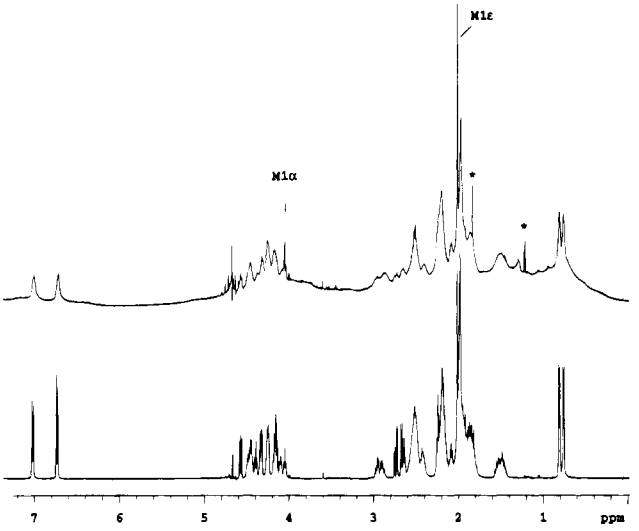

FIGURE 5: 1D ^{1}H NMR spectra of B3P, shown at the bottom, and B3P complexed with aldolase (70 μM), shown at the top. Differential line broadening is observed upon addition of aldolase showing specific binding. The H_α and methyl (H_ϵ) resonances of M1, indicated by arrows, remain narrow with respect to other resolved resonances, indicating that the N-terminus is conformationally mobile in the bound state (2.8 mM B3P, 10 mM PO_4, pH 5.5, 25 °C). Impurities are denoted with an asterisk.

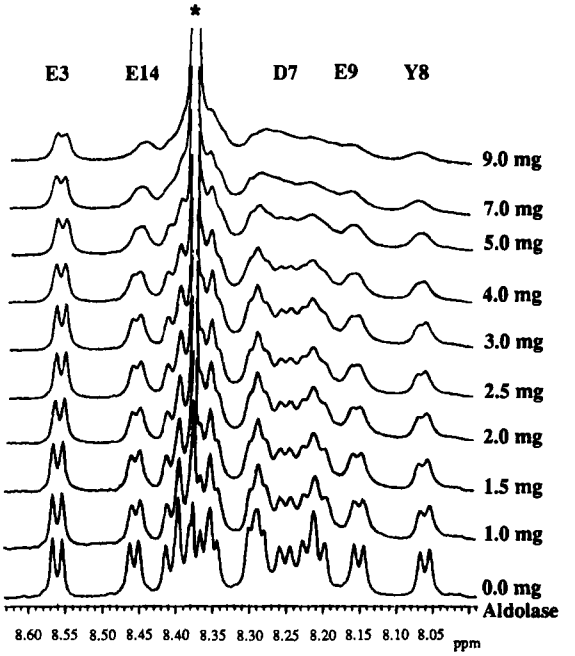

FIGURE 6: 1D ^{1}H NMR spectra showing the H_N chemical shift region for titration of B3P with aldolase (2.8 mM B3P, 10 mM PO_4, pH 5.5, 25 °C). For the sample containing 9 mg of aldolase (80 μM), the mole ratio is 8.75 B3P to 1 aldolase monomer. Differential line broadening is observed for B3P resonances as aldolase is added. E3 shows a slower rate of broadening, suggesting backbone mobility or conformational heterogeneity at the N-terminus while D7, Y8, and E9 show faster rates of line broadening, indicating decreased mobility in the bound state. The asterisk indicates an impurity.

molar equiv of aldolase subunit. It is seen that the ^{1}H resonances of B3P exhibit varying degrees of line broadening when B3P is in the presence of aldolase. As an example, the H_α proton and methyl group of M1 show only slight broadening compared with other proton resonances, so M1 is more mobile or has greater conformational heterogeneity in the bound state. Further evidence of differences in binding interactions is shown from a titration study (Figure 6). As B3P was titrated with aldolase, the rate of H_N line broadening was analyzed for protons that were resolved. The data show that H_N protons of residues such as E3 near the N-terminus of B3P have slower rates of line-width broadening than D7, Y8, and E9. Thus, the parts of B3P involving strong interactions with aldolase according to the titration are residues flanking and including Y8. This pattern of line broadening is consistent with the ET-NOESY data showing many short interproton distances within the defined loop of bound B3P and the lack of NOE's at the N-terminus. In contrast, the C-terminus also lacks NOE's, yet H_N of E14 shows a rate of broadening comparable to that of D7, Y8, and E9.

DISCUSSION

A Proposed Binding Site for B3P on Aldolase. In order to define the interaction of band 3 when it is bound to aldolase, obviously one must define the binding site for band 3 on aldolase. Although to date direct structural evidence for this binding site is unavailable, based on stoichiometry

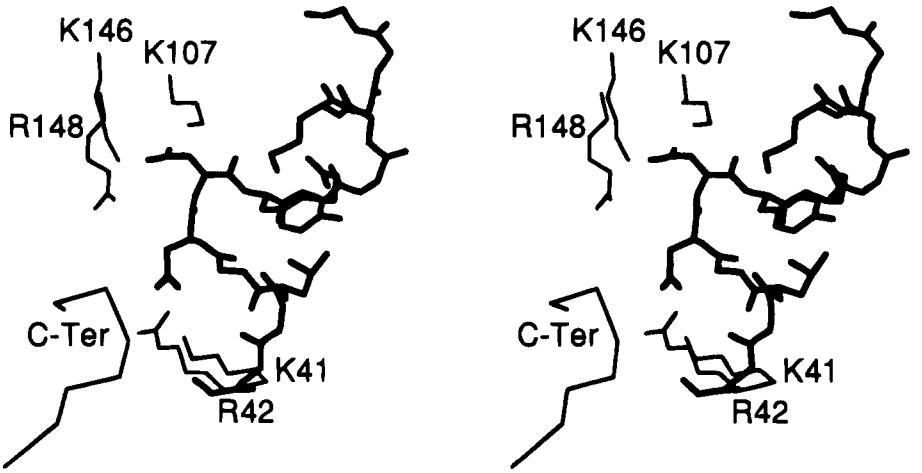

FIGURE 7: Stereoview of the modeled B3P–aldolase complex. B3P (thick lines) forms complementary charge pairs with the highly conserved residues K107, K146, R148, and R42 in the active site pocket of aldolase (thin lines). The N-terminus of B3P is in close proximity to the C-terminus of aldolase, a highly mobile region of aldolase based on the crystallographic *B*-values (Gamblin et al., 1990). This proximity to a flexible region of aldolase could account for the NMR conformational disorder.

measurements and inhibition studies of this system as well as the NMR structural results for B3P, we propose that the binding site for B3P is the catalytic site of aldolase. First, biochemical and kinetic evidence for specific binding of B3P to the catalytic site is revealed by stoichiometry measurements and aldolase inhibition assays (Schneider et al., unpublished results). Sephadex displacement experiments show that B3P binds aldolase with a molar ratio of 4:1. Since aldolase is a tetramer with four identical active sites, this stoichiometry is consistent with one molecule of B3P binding to each catalytic site of aldolase. There is also evidence that band 3 binds to aldolase with a molar ratio of 4:1 (Schubert et al., 1992). Furthermore, aldolase inhibition assays show that B3P (Schneider et al., unpublished results) and band 3 in ghost cells (Strapazon & Steck, 1977; Murthy et al., 1981) compete with substrate binding. Second, it was shown here that B3P bound to aldolase is displaced by dihydroxyacetone phosphate, which binds specifically to the active site of aldolase. Finally, B3P is a very acidic peptide, and it has been shown that binding is largely electrostatic in nature (Strapazon & Steck, 1977). The B3P structure as described previously in Results showed that the side-chain carboxylates of D6, D7, and E9 form an area of negative charge density on the outer face of the peptide loop that would be attracted to a broad area of positive charge. A location on aldolase that meets this criterion is the catalytic site. Several basic residues in the catalytic site of aldolase including R42, K107, K146, R148, and K229 are highly conserved in all type I aldolases sequenced to date and are thought to orient fructose 1,6-bisphosphate for the cleavage reaction (Sygusch et al., 1987; Malek et al., 1988; Morris & Tolan, 1994). Therefore, B3P interacts with the active site residues in a very complementary fashion.

Intermolecular Docking of B3P in the Aldolase Active Site. It is important to evaluate a number of NMR structures for modeling the B3P–aldolase complex given the conformational heterogeneity described above. Consequently, B3P was modeled in the active site of human muscle aldolase (Gamblin et al., 1990) by an intermolecular docking procedure that takes into account multiple B3P structures, as described in Materials and Methods. All 20 final B3P structures were individually docked onto the aldolase monomer. Restrained energy minimization and molecular dynamics allowed B3P to interact with the aldolase active site region and its perimeter to assume a position that was both electrostatically and sterically favorable. The mean intermolecular interaction energy and mean number of NOE violations exceeding a 0.1 Å cutoff were -540 ± 97 kcal/mol and 4.5 ± 1.3 violations, respectively. Furthermore, the mean NOE violation with a 0.2 Å cutoff was 0.47 ± 0.84 violation, showing that the majority of these NOE violations are relatively minor. The mean pairwise rmsd for main-chain atoms from L4 to E9 of B3P was 1.08 ± 0.42 Å for the 20 docked B3P structures, whereas it was 1.21 ± 0.5 Å before docking. This indicates further convergence toward a common B3P conformation when docked with aldolase. Each B3P molecule in the corresponding B3P–aldolase coordinate set was screened on the basis of low intermolecular interaction energy, few NOE violations, and whether ϕ and ψ angles were found in acceptable regions in a Ramachandran plot. A B3P–aldolase coordinate set that scored well in all three categories was chosen out of the 20 complexes for further analysis and discussed in detail here. This complex, referred to hereafter as the B3PALD complex, has an intermolecular interaction energy equal to -643 kcal/mol, and the B3P structure had zero NOE violations exceeding a 0.2 Å cutoff.

The modeled B3PALD complex is shown in Figures 7 and 8A. The B3P loop (residues 4–9) extends into the β-barrel of aldolase which contains the active site residues and other highly conserved regions (Figure 7). Binding is primarily electrostatic in nature (Figure 8A) with the side-chain carboxylates of D6 and D7 interacting with conserved arginine and lysine residues. The side-chain carboxylate of D6 interacts with the side chains of K41 and R42 of aldolase while the side-chain carboxylate of D7 interacts with the side chains of K107, K146, and R148. Aldolase residues K41, R42, and K107 have all been implicated as the 1-phosphate binding site for the substrate, fructose 1,6-bisphosphate, while Lys 146 and Arg 148 compose the 6-phosphate binding site (Shapiro et al., 1968; Anai et al., 1973; Hartman & Brown, 1976; Palczewksi et al., 1985; Gamblin et al., 1991). B3P also shares a number of other intermolecular ionic interactions and hydrogen bonds with aldolase as seen in Table 1,

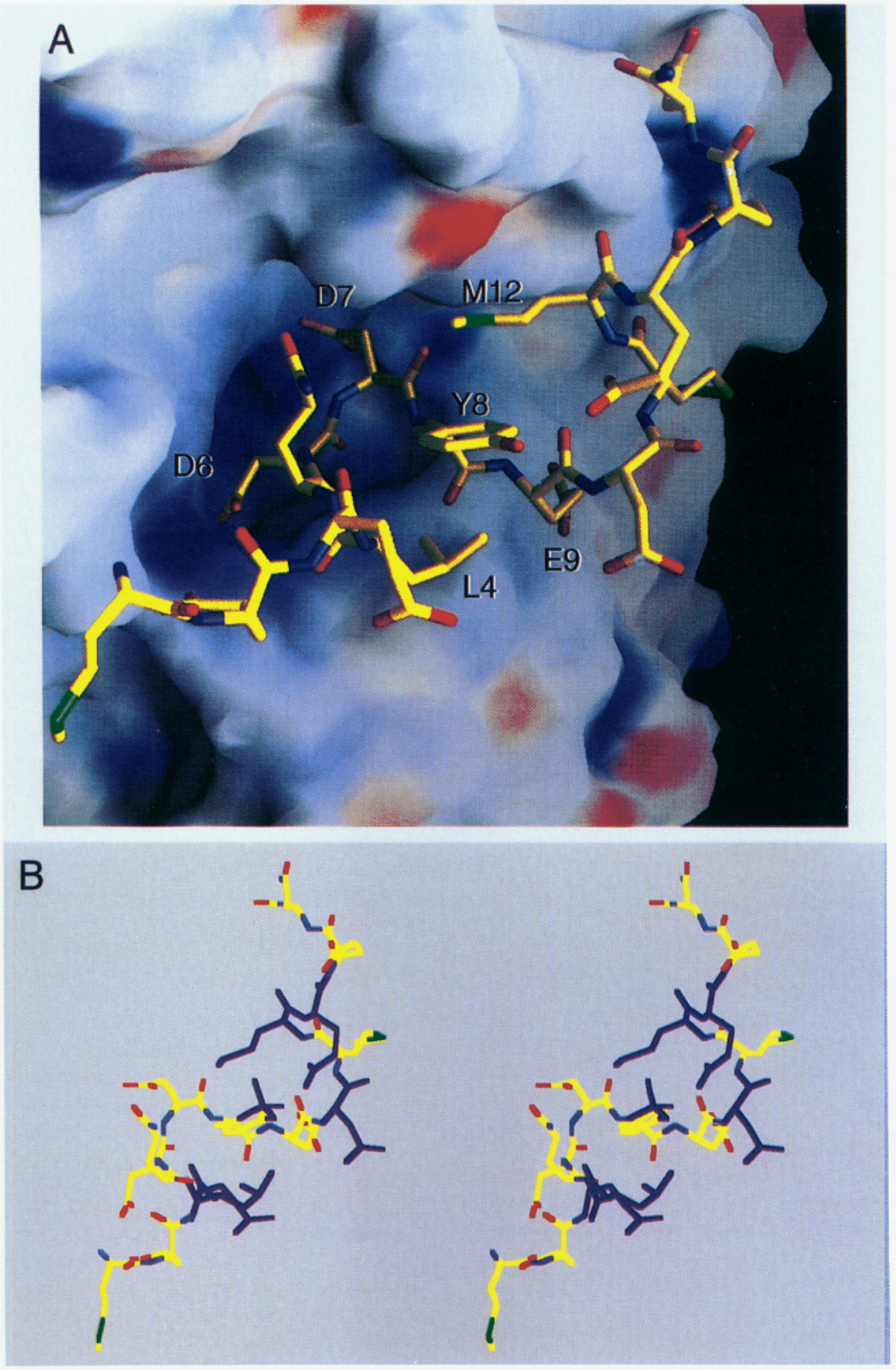

FIGURE 8: (A) Model B3P−aldolase complex which includes electrostatic binding interactions as shown by the electrostatic potential surface map of aldolase. Blue regions on the surface are electropositive, and red regions are electronegative. The B3P loop forms a complementary fit with the active site pocket of aldolase. B3P residues D6 and D7 extend into the active site where highly conserved lysine and arginine residues exist. The positively charged N-terminus of B3P is in close proximity with an electropositive area on aldolase, which likely contributes to its mobility. This figure was generated by the GRASP program (Nicholls et al., 1991). (B) Stereoview of B3P from the model complex with a phosphoryl group built onto Y8 in order to better understand why phosphorylation disrupts aldolase inhibition. During rotation of the phosphate, electrostatic and steric repulsion is encountered from the B3P residues that are highlighted in purple. This view shows the lowest energy phosphate rotamer (+100°).

including the following: M1−S359, N360; E2−K41; L4−K41; E9−T36; M12−Q125; E14−K110; N15−Q125, D128.

The structural studies and model for binding we propose correlate well with the NMR and biochemical evidence, in

Table 1: Intermolecular Ionic Interactions and Hydrogen Bonds from the B3PALD Model Complex[a]

B3P		aldolase		O−N or O−O
residue	atom	residue	atom	distance (Å)
M1	H_T2[b]	S359	Oγ	2.97
M1	H_T2	N360	Oδ1	2.89
M1	H_T3	S359	Oγ	2.97
E2	Oε1	K41	Hζ2	2.63
L4	O	K41	Hζ1	2.93
D6	Oδ2	K41	Hζ3	2.75
D6	Oδ1	R42	Hη12	2.63
D6	Oδ1	R42	Hη21	2.69
D7	Oδ1	K107	Hζ2	2.62
D7	Oδ1	K146	Hζ1	2.65
D7	Oδ2	R148	He	2.72
D7	Oδ2	R148	Hη22	2.73
E9	Oε1	T36	H_N	2.78
E9	Oε1	T36	Hγ1	2.64
M12	O	Q125	Hε21	2.95
E14	Oε2	K110	Hζ2	2.62
N15	Hδ21	Q125	Oε1	3.15
N15	Hδ21	D128	Oδ2	3.23
N15	Hδ22	D128	Oδ2	3.23

	⟨energy⟩[c] (kcal/mol)
M1−E3	−36.65 ± 42.24
L4−E9	−391.13 ± 64.25
E13−N15	−80.43 ± 69.83

[a] Ionic interactions and hydrogen bonds were determined with the QUANTA program. The cutoff distance was 3.5 Å. [b] H_T designates hydrogens from the N-terminal amine. [c] The interaction energy (van der Waals plus electrostatics) between the segment of B3P and aldolase is averaged over the 20 complexes modeled from the 20 B3P NMR structures and human aldolase (Gamblin et al., 1990).

support of B3P inhibiting aldolase by binding in the catalytic site of each subunit to interfere with substrate cleavage. The differential binding effects for parts of B3P can be understood from the extent of intermolecular interactions in the B3PALD complex. The model of the complex shows multiple ionic interactions and hydrogen bonds between D6, D7, or E9 of B3P and aldolase residues in the active site, consistent with the broader H_N resonances in the titration shown in Figure 6 and a single mode of binding for the region of B3P immediately surrounding Y8. The titration results for E14 also show relatively slow backbone motion at the C-terminus of B3P, consistent with the favorable interactions between E14 or N15 of B3P and aldolase. The structural disorder in the C-terminus from the NMR structure determination is due to the small number of NOE restraints. From the fact that H_N of E14 broadens early in the titration yet has a paucity of NOE interactions, it is concluded that the conformation of the C-terminus of B3P binds on the protein surface in an extended conformation with strong interactions with aldolase either in a single mode lacking short interresidue $^1H-^1H$ distances or in multiple modes apparent from the set of NMR structures. In regard to the N-terminus the intermolecular interactions in the model and structural mobility apparent from the NMR line widths of M1 and E2 seem to be contradictory; in the model, the N-terminus of B3P is also hydrogen bonded to aldolase, yet the relatively narrow resonances for E3 and M1 reflect a certain conformational heterogeneity in the complex. Furthermore, there is heterogeneity in the NMR structure solution since few NOE's are observed for the N-terminus of B3P. The proposed complex model explains the NMR results in the following manner. The N-terminus of B3P contacts the C-terminus of aldolase (Figure 7), which has relatively high *B*-factors determined from the crystallographic study due to a hinge region with high flexibility (Sygusch et al., 1987; Gamblin et al., 1990). It has been suggested that the C-terminus is responsible for the various differences in substrate specificity among all type I aldolases (Sygusch et al., 1987). Since the N-terminal portion of B3P interacts with the C-terminus of aldolase, flexibility of the C-terminus could increase the overall motion, or structural heterogeneity, of the N-terminus of B3P in the complex. In addition, the model places the N-terminal amine of B3P in close spatial proximity to positive charges on aldolase (Figure 8A), especially from the side chain of K41, such that charge repulsion would weaken binding and cause disorder at the N-terminus. This repulsion also explains the fact that B3P with a free N-terminus binds aldolase with lower affinity than the N-terminally blocked B3P (Murthy et al., 1981; Wang et al., 1992). Finally, the correspondence between the model and experimental observations is further validated by averaging the total intermolecular energy over the 20 modeled complexes. The van der Waals and electrostatic terms were calculated between aldolase and a specified region of B3P. The average intermolecular energies between aldolase and the B3P regions M1−E3, L4−E9, and E13−N15 are −36.65 ± 42.24, −391.13 ± 64.25, and −80.43 ± 69.83 kcal/mol, respectively. Thus, the N-terminus binds more weakly than the C-terminus while the loop structure interacts more strongly than either terminal portion of B3P.

Blocking B3P−Aldolase Association through Tyrosine 8 Phosphorylation. When tyrosine 8 of human erythrocyte band 3 is phosphorylated, aldolase inhibition is disrupted and full catalytic activity returns (Low et al., 1987). Low and co-workers (1987) believe the nature of this disruption is primarily due to electrostatic repulsion since B3P possesses a large, net negative charge, and addition of a phosphate could reasonably be predicted to destabilize the bound conformation. In the NMR structure of unphosphorylated B3P, the folding of the loop about Y8 does leave an empty pocket that could accommodate a phosphate, but the phosphoryl group would result in a strong electrostatic repulsion with other B3P residues. In order to confirm intramolecular electrostatic repulsion as the major destabilizing factor of this loop structure, a phosphoryl group was modeled onto Y8 (Figure 8B), and the interaction energy between the phosphate moiety and B3P or aldolase was calculated as a function of dihedral rotation. (CHARMM version 23 parameter and topology files were modified to include a phosphorylated tyrosine.) The phosphoryl group was rotated about the $C_\zeta - O_\eta$ bond in Y8 while the remainder of the molecule remained fixed. For each 20° rotation of the phosphoryl group, the interaction energy between the phosphate and the rest of the B3P or aldolase molecule was calculated. For comparison, the hydroxyl moiety of Y8 was treated in an identical fashion as the phosphate, and the interaction energies were calculated between the hydroxyl moiety and the rest of B3P. The electrostatic and van der Waals contributions to the interaction energy as a function of rotation angle in the B3PALD complex are represented as energy curves shown in Figure 9. While a hydroxyl moiety of Y8 for nearly all rotation angles has favorable interactions with the rest of the B3P molecule (negative electrostatics and virtually no steric repulsion), a phosphate moiety is destabilizing at all rotation angles. B3P residues having unfavor

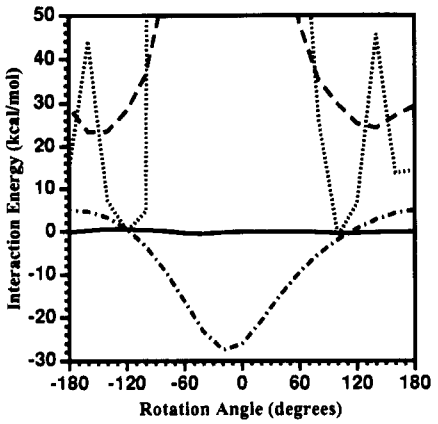

FIGURE 9: Plot of interaction energy as a function of phosphate or hydroxyl rotation for B3P phosphorylated at Y8, indicating that intramolecular electrostatic repulsion is the major contributor to disruption of aldolase inhibition. Intramolecular effects of phosphorylation: (···) denotes van der Waals repulsion while (- - -) shows the electrostatic interaction energy between phosphate and B3P. Intermolecular effects of phosphorylation: (—) indicates the electrostatic energy between phosphate and aldolase. Comparison for unphosphorylated B3P: (—·—) shows the electrostatic energy between the Y8 hydroxyl moiety and B3P.

able interactions with the phosphate moiety are shown in purple in Figure 8B. The phosphate can be sterically accommodated in the conformation shown in Figure 8B (see the +100° rotamer in Figure 9); however, all phosphate rotamers have high electrostatic energy because of intramolecular effects. The side-chain carboxylates of E3, D10, and E13 are the source of the repulsive electrostatic character of the interaction. For rotamers with large, positive van der Waals energy, contacts occur with the L4 side chain, D10 backbone, and M12 methyl group. One can clearly see from Figure 9 that intramolecular electrostatic repulsion prevails regardless of the phosphate orientation. B3P is held fixed during the phosphate rotation, but it is not likely that energy minimization could completely eliminate the electrostatic repulsion due to E3, D10, and E13 while maintaining the loop structure of residues 4–9. In regard to the intermolecular effects of phosphorylation, van der Waals and electrostatic interactions between the phosphate moiety and aldolase are slightly favorable for many of the phosphate orientations since the negatively charged phosphate group and the active site, lined with positive charges, lead to attractive electrostatic energy.

Overall, this analysis suggests that intramolecular electrostatic repulsion via phosphorylation of Y8 is the major factor blocking the formation of the B3P–aldolase complex. Intermolecular interactions with aldolase, in particular B3P residues D6 and D7 which are key for recognition and binding, play a negligible role in preventing formation of the complex after phosphorylation.

A mechanism whereby phosphorylation destabilizes the loop structure due to intramolecular effects and prevents the formation of the complex, as proposed here for B3P–aldolase, could have general application to other biological systems. Tyrosyl phosphorylation prevents formation of the band 3–aldolase complex concluded from this model because a conformation with band 3 folded around Y8 is unable to form due to intramolecular electrostatic repulsion. Thus, phosphorylated band 3 is not able to inhibit aldolase activity and leads to elevated human erythrocyte glycolysis levels. Disruption of protein–protein association by phosphorylation has been reported for other proteins (Nishikawa et al., 1985; Benovic et al., 1986; Gould & Nurse, 1989; Reizer et al., 1992), but insufficient structural information is available to determine if the mechanism proposed for the band 3–aldolase complex is relevant to these biological systems. However, isocitrate dehydrogenase is a case where phosphorylation disrupts protein function, and structural information (Hurley et al., 1990; Dean & Koshland, 1990) has elucidated the mechanism. The mechanism for isocitrate dehydrogenase involves direct conflict with substrate binding by a phosphorylated active site serine. Disruption of the protein–protein interaction in the band 3-glycolytic enzyme complexes is unlike many phosphorylation events which promote protein–protein interactions, such as complexes involving SH2 domains. We also note that binding the tyrosyl–peptide of band 3 requires a folded conformation, whereas phosphopeptides bind to SH2 domains in an extended conformation (Waksman et al., 1992; Xu et al., 1995; Stanfield & Wilson, 1995).

CONCLUSIONS

In this paper, we have reported the three-dimensional solution structure of B3P, the 15 N-terminal residues of human erythrocyte band 3, when bound to rabbit muscle aldolase in solution. The final 20 structures determined using exchange-transferred NOESY data have negative energy and a low number of NOE violations. The major structural feature observed from the NMR structure of B3P involves a loop from L4 through E9 which folds around Y8, the phosphorylation site. The peptide termini are structurally heterogeneous, both as a result of the structure determination and as shown by differential NMR line broadening. Intermolecular docking of B3P in the active site of aldolase shows that B3P is able to form extensive intermolecular ionic interactions between the B3P loop and conserved active site lysine and arginine residues of aldolase. It was shown that if a phosphate is built onto Y8 in this modeled B3PALD complex, intramolecular electrostatic repulsion destabilizes the folded conformation of B3P, which could reasonably be the cause for disrupting aldolase inhibition and elevation of human erythrocyte glycolysis. In order to further understand the interaction of band 3 with the glycolytic enzymes it inhibits, NMR structure determination is currently in progress with the B3P–GAPDH complex. It is of interest to see if B3P inhibits all three enzymes through a common binding motif. The mechanism presented here for blocking protein–protein association by intramolecular electrostatic destabilization of the tyrosyl loop conformation could occur in other phospho–tyrosyl systems as well. Is there a phospho–tyrosyl signaling pathway regulating human erythrocyte glycolysis? We have presented a structural foundation for this regulation. Discovery of a component that triggers the phosphorylation–dephosphorylation event would help to answer this question.

ACKNOWLEDGMENT

The authors thank Dr. Philip S. Low, Chemistry Department, Purdue University, for useful discussions about band 3 and Dr. Jie Zheng for discussions about the exchange-transferred NOE method and helpful suggestions for protein preparation.

SUPPORTING INFORMATION AVAILABLE

A table containing the ^1H chemical shift assignments for B3P in the free state and the X-PLOR distance restraints file for B3P in the bound state (3 pages). Ordering information is given on any current masthead page.

REFERENCES

Anai, M., Laai, C. Y., & Horecker, B. L. (1973) *Arch. Biochem. Biophys. 156*, 712−719.

Balaram, P., Bothner-By, A. A., & Breslow, E. (1973) *Biochemistry 12*, 4695−4704.

Bax, A., & Davis, D. G. (1985) *J. Magn. Reson. 65*, 355.

Benovic, J. L., Strasser, R. H., Caron, M. G., Lefkowitz, R. J. (1986) *Proc. Natl. Acad. Sci. U.S.A. 83*, 2797−2801.

Billeter, M., Braun, W., & Wuthrich, K. (1982) *J. Mol. Biol. 155*, 321−346.

Boivin, P., & Galand, C. (1986) *Biochem. Biophys. Res. Commun. 134*, 557−564.

Boivin, P., Galand, C., & Bertrand, O. (1986) *Biochim. Biophys. Acta 860*, 243−252.

Bothnerby, A. A., Stephens, R. L., Lee, J.-M., Warren, C. D., & Jeanloz, R. W. (1984) *J. Am. Chem. Soc. 106*, 811−813.

Braunschweiler, L., & Ernst, R. R. (1983) *J. Magn. Reson. 55*, 521−525.

Brooks, B. R., Bruccoleri, R. E., Olafson, B D., States, D. J., Swaminathan, S., & Karplus, M. (1983) *J. Comput. Chem. 4*, 187−217.

Brünger, A. T. (1992) *X-PLOR 3.1: A System for X-ray Crystallography and NMR*, Yale University Press, New Haven, CT.

Campbell, A. P., & Sykes, B. D. (1993) in *Annual Review of Biophysical and Biomolecular Structure* (Engleman, D. M., Cantor, C. R., & Pollard, T. D., Eds.) pp 99−122, Annual Reviews Inc., Palo Alto, CA.

Clore, G. M., & Gronenborn, A. M. (1982) *J. Magn. Reson. 48*, 402−417.

Clore, G. M., & Gronenborn, A. M. (1983) *J. Magn. Reson. 53*, 423−442.

Clore, G. M., Robien, M. A., & Gronenborn, A. M. (1993) *J. Mol. Biol. 231*, 82−102.

Dean, A. M., & Koshland, D. E., Jr. (1990) *Science 249*, 1044−1046.

Espenson, J. H. (1981) in *Chemical Kinetics and Reaction Mechanisms* (Espenson, J. H., Ed.) pp 168−170, McGraw-Hill Inc., New York.

Gamblin, S. J., Cooper, B., Millar, J. R., Davies, G. J., Littlechild, J. A., & Watson, H. C. (1990) *Fed. Eur. Biochem. Soc. Lett. 262*, 282−286.

Gamblin, S. J., Davies, G. J., Grimes, J. M., Jackson, R. M., Littlechild, J. A., & Watson, H. C. (1991) *J. Mol. Biol. 219*, 573−576.

Gould, K. L., & Nurse, P. (1989) *Nature 342*, 39−45.

Harrison, M. L., Rathinavelu, P., Arese, P., Geahlen, R. L., & Low, P. S. (1991) *J. Biol. Chem. 266*, 4106−4111.

Harrison, M. L., Isaacson, C. C., Burg, D. L., Geahlen, R. L., & Low P. S. (1994) *J. Biol. Chem. 269*, 955−959.

Hartman, F. C., & Brown, J. P. (1976) *J. Biol. Chem. 251*, 3057−3062.

Hurley, J. H., Dean, A. M., Sohl, J. L., Koshland, D. E., Jr., & Stroud, R. M. (1990) *Science 249*, 1012−1016.

Jeener, J., Meier, B. H., Bachmann, P., & Ernst, R. R. (1979) *J. Chem. Phys. 71*, 4546−4553.

Jenkins, J. P., Madden, D. P., & Steck, T. L. (1984) *J. Biol. Chem. 259*, 9374−9378.

Kessler, H., Griesinger, C., Kerssebaum, R., Wagner, K., & Ernst, R. R. (1987) *J. Am. Chem. Soc. 109*, 607−609.

Lee, W., & Krishna, N. R. (1992) *J. Magn. Reson. 98*, 36−48.

London, R. E., Perlman, M. E., & Davis, D. G. (1992) *J. Magn. Reson. 97*, 79−98.

Low, P. S. (1986) *Biochim. Biophys. Acta 864*, 145−167.

Low, P. S., Allen, D. P., Zioncheck, T. F., Chari, P., Willardson, B. M., Geahlen, R. L., & Harrison, M. L. (1987) *J. Biol. Chem. 262*, 4592−4596.

Low P. S., Rathinavelu, P., & Harrison, M. L. (1993) *J. Biol. Chem. 268*, 14627−14631.

MacKerell, A. D., Jr., Bashford, D., Bellott, M., Dunbrack, R. L., Jr., Field, M. J., Fischer, S., Gao, J., Guo, H., Ha, S., Joseph, D., Kuchnir, L., Kuczera, K., Lau, F. T. K., Mattos, C., Michnick, S., Ngo, T., Nguyen, D. T., Prodhom, B., Roux, B., Schlenkrich, M., Smith., J. C., Stote, R., Straub, J. Wiorkiewicz-Kuczera, J., & Karplus, M. (1992) *FASEB J. 6*, A143.

Macura, S., & Ernst, R. R. (1980) *Mol. Phys. 41*, 95−117.

Malek, A. A., Hy, M., Honegger, A., Rose, K., & Brenner-Holzach, O. (1988) *Arch. Biochem. Biophys. 266*, 10−31.

Mehler, A. H., & Bloom, B. (1963) *J. Biol. Chem. 238*, 105−107.

Mohamed, A. H., & Steck, T. L. (1986) *J. Biol. Chem. 261*, 2804−2809.

Morris, A. J., & Tolan, D. R. (1994) *Biochemistry 33*, 12291−12297.

Murali, N., Gotam, K. J., Landy, S. B., & Nageswara Rao, B. D. (1993) *Biochemistry 32*, 12941−12948.

Murali, N., Jarori, G. K., & Nageswara Rao, B. D. (1994) *Biochemistry 33*, 14227−14236.

Murthy, S. N. P., Liu, T., Kaul, R. K., Kohler, H., & Steck, T. L. (1981) *J. Biol. Chem. 256*, 11203−11208.

Ni, F. (1994) *Progr. NMR Spectrosc. 26*, 517−606.

Ni, F., & Zhu, Y. (1994) *J. Magn. Reson. B103*, 180−184.

Nicholls, A., Sharp, K. A., & Honig, B. (1991) *Proteins: Struct., Funct., Genet. 11*, 281−296.

Nishikawa, M., Shirakawa, S., & Adelstein, R. S. (1985) *J. Biol. Chem. 260*, 8978−8983.

Palczewski, K., Hargrave, P. A., Folta, E. J., & Kochman, M. (1985) *Eur. J. Biochem. 146*, 309−314.

Post, C. B., Meadows, R. P., & Gorenstein, D. G. (1990) *J. Am.Chem. Soc. 112*, 6796−6803.

Reizer, J., Sutrina, S. L., Wu, L.-F., Deutscher, J., Reddy, P., & Saier, M. H., Jr. (1992) *J. Biol. Chem. 267*, 9158−9169.

Rogalski, A. A., Steck, T. L., & Waseem, A. (1989) *J. Biol. Chem. 264*, 6438−6446.

Salhany, J. M. (1990) in *Erythrocyte Band 3 Protein* (Salhany, J. M., Ed.) pp 153−177, CRC Press Inc., Boca Raton, FL.

Schubert, D., Huber, E., Lindenthal, S., Mulzer, K., & Schuck, P. (1992) in *Progress In Cell Research 2* (Bamberg, E., & Passow, H., Eds.) pp 209−217, Elsevier Science Publishers, Amsterdam, The Netherlands.

Shapiro, S., Enser, M., Pugh, E., & Horecker, B. L. (1968) *Arch. Biochem. Biophys. 128*, 554−562.

Stanfield, R. I., & Wilson, I. A. (1995) *Curr. Opin. Struct. Biol. 5*, 103−113.

States, D. J., Haberkorn, R. A., & Ruben, D. J. (1982) *J. Magn. Reson. 48*, 286−292.

Strapazon, E., & Steck, T. L. (1976) *Biochemistry 15*, 1421−1424.

Strapazon, E., & Steck, T. L. (1977) *Biochemistry 16*, 2966−2971.

Sygusch, J., Boulet, H., & Beaudry D. (1985) *J. Biol. Chem. 260*, 15286−15290.

Sygusch, J., Beaudry, D., & Allaire M. (1987) *Proc. Natl. Acad. Sci. U.S.A. 84*, 7846−7850.

Tanner, M. J. A., Martin, P. G., & High, S. (1989) *Biochem. J. 256*, 703.

Tsai, I. H., Murthy, S. N. P., & Steck, T. L. (1982) *J. Biol. Chem. 257*, 1438−1442.

Wagner, G., & Wuthrich, K. (1982) *J. Mol. Biol. 155*, 347−366.

Waksman, G., Kominos, D., Robertson, S. C., Pant, N., Baltimore, D., Birge, R. B., Cowburn, D., Hanafusa, H., Mayer, B. J., Overduin, M., Resh, M. D., Rios, C. B., Silverman, L., & Kuriyan, J. (1992) *Science 358*, 646−653.

Wang, C. C., Badylak, J. A., Lux, S. E., Moriyama, R., Dixon, J. E., & Low, P. S. (1992) *Protein Sci. 1*, 1206−1214.

Wuthrich, K., Wider, G., Wagner, G., & Braun, W. (1982) *J. Mol. Biol. 155*, 311−319.

Xu, R. X., Word, M., Davis, D. G., Rink, M. J., Willard, D. H., Jr., & Gampe, R. T., Jr. (1995) *Biochemistry 34*, 2107−2121.

Zheng, J., & Post, C. B. (1993) *J. Magn. Reson. 101*, 262−270.

BI9516438